

Structural, Optical and Photocatalytic Properties of Ba-Doped TiO₂ Thin Films

A. DOULA*, R. BENSAHA AND O. BELDJEBLI

Laboratoire de Céramiques, Faculté des Sciences Exactes, Université Frères Mentouri-Constantine1, Route Ain El Bey, 25000 Constantine, Algeria

Received: 20.08.2021 & Accepted: 13.11.2021

Doi: [10.12693/APhysPolA.140.421](https://doi.org/10.12693/APhysPolA.140.421)

*e-mail: doulaaicha1112@gmail.com

Ba-doped TiO₂ thin films were deposited onto glass substrates by sol-gel spin-coating method and annealed at 550°C for 2 h. The effect of barium doping on the structural, morphological, optical, and photocatalytic properties of TiO₂ thin films was investigated. X-ray diffraction analysis revealed that all films crystallize in the anatase phase with the plane (101) as preferential orientation. As a result of the Ba doping, the crystallite size decreased from 19 to 9 nm. The surface morphology and roughness of TiO₂ were shown to be affected by Ba doping content using atomic force microscopy. As Ba content increased, the optical transmittance of the films increased to over 85% in the visible region and the gap energy increased from 3.42 to 3.77 eV. Doping by barium enhances the photocatalytic activity of TiO₂ film for degradation of rhodamine B under UV light irradiation, and the best performance was found for 3% of Ba:TiO₂ film.

topics: TiO₂ thin films, Ba doping, spin-coating, photocatalytic activity

1. Introduction

Because of advances in semiconductor material research, the degradation of organic pollutants in water via heterogeneous photocatalysis has improved. Titanium dioxide (TiO₂) is the most likely candidate to enhance photocatalytic activity due to its special properties such as high activity, chemical stability and environmental friendliness [1]. TiO₂ is composed of three crystalline phases: anatase, brookite, and rutile phase, among which the anatase phase demonstrates high photocatalytic activity. Controlling the physical properties of TiO₂, such as grain size to achieve a high surface area, can improve its photocatalytic properties and increase its efficiency in the degradation of a wide range of organic pollutants [3, 4]. Furthermore, the addition of metallic or non-metallic elements would act as traps for photoinduced electrons and holes, delaying electron-hole recombination.

Titanium dioxide TiO₂ powder catalyst development has piqued the interest of researchers [5, 6]. However, there are some drawbacks to its subsequent use, such as catalyst separation after each run and stirring during the reaction, as well as limited light distribution. Thus, the preparation of a thin film catalyst will overcome these drawbacks, and also broaden the applications of catalyst to antibacterial ceramic tiles and self-cleaning glasses [7]. Among thin film deposition methods, the sol-gel

spin-coating is the simplest, most cost-effective, and has numerous advantages, e.g. TiO₂ adheres easily to substrates. The deposition of TiO₂ thin film by the sol-gel method has been reported by few authors [7–10].

To the best of our knowledge, the photocatalytic properties of Ba-doped TiO₂ as a thin film have not been reported. In this paper, we present a comparative study on the photocatalytic efficiency of undoped and Ba-doped TiO₂ thin films prepared by the sol-gel spin-coating method, as well as the optical and morphological structure. Under the ultraviolet light irradiation, the photocatalytic behavior of Ba-doped TiO₂ thin films in the removal of RhB pollutants in wastewater was investigated.

2. Experimental

2.1. Films preparation

We used 1 mol of butanol (C₄H₉OH) as a solvent, 4 mol of acetic acid (CH₃COOH) as a catalyst, 1 mol of distilled water, and 1 mol of tetrabutyl-orthotitanate Ti(C₄H₉O)₄ was added to the mixture as an organic source of titanium [11, 12]. To precipitate undoped and Ba-doped, TiO₂ thin films were deposited by sol-gel spin-coating method on glass substrates. We then have melted different ratios of acetate barium (C₄H₆BaO₄) in TiO₂ solution. Finally, these solutions were stirred for 6 h

at room temperature to obtain homogeneous solutions of TiO₂ doped with 1%, 3%, 5% and 7% of Ba. These solutions were spin-coated on the substrates with a speed of 3000 rpm for 30 s. After each coating, the samples were dried at temperature $\simeq 100^\circ\text{C}$ for 10 min. This process of coating and heating was repeated 6 times. At last, the samples were annealed at 550°C for 2 h.

2.2. Photocatalytic procedure

To evaluate the photocatalytic activity of Ba-doping TiO₂ thin films, we followed the degradation of rhodamine B (RhB) solution (10^{-5} mol/l) under the ultraviolet light source (VL-215. LC, 15 W and $\lambda = 365$ nm), with emission light of 365 nm. Samples of TiO₂ doped with 0%, 1%, 3%, 5%, and 7 % of barium were placed in a flask containing 25 ml of an aqueous solution. After that, the distance between the film and the lamp was fixed to 11 cm. Every 30 min, 4 ml of the was withdrawn, and the RhB concentration was determined using UV Spectroscopy (JASCO) by observing the peak absorption at about 554 nm for 180 min.

2.3. Films characterization

The structural properties were characterized using a Panalytical-Empyrean X-ray diffractometer (XRD) in grazing incidence mode with Cu K_α radiation ($\lambda_{Cu} = 1.54056$ Å). Optical transmission was performed by a JASCO UV-Vis spectrophotometer. In addition, film surface morphology was observed using an Asylum research (BRUKER ICON SCAN ASYST) and atomic force microscopy (AFM).

3. Results and discussion

3.1. Structural properties

The XRD patterns of undoped and doped TiO₂ thin films with various Ba contents annealed at 550°C for 2 h are shown in Fig. 1. We notice the presence of peaks corresponding to the planes (101), (004), (200), (105) and (211) of the anatase phase (JCPDS 21-1272). It can be seen that the intensity of all the diffraction peaks decreases as a function of Ba doping, indicating that the film crystallinity decreases. Furthermore, no peak related to barium oxide was found in all spectra, which is more likely due to the low content of Ba doping.

Moreover, the crystallite size (L) of undoped and Ba-doped TiO₂ thin films can be deduced from XRD broadening peak of (1 0 1) using the Scherrer equation [13]

$$L = \frac{0.94\lambda}{\beta \cos(\theta)}, \quad (1)$$

where L is the crystallite size [nm], λ is the wavelength of X-ray ($\lambda_{Cu K_\alpha} = 1.54056$ Å), β [rad] is the full width at half maximum (FWHM) of the (1 0 1) diffraction peak, and θ is the Bragg angle.

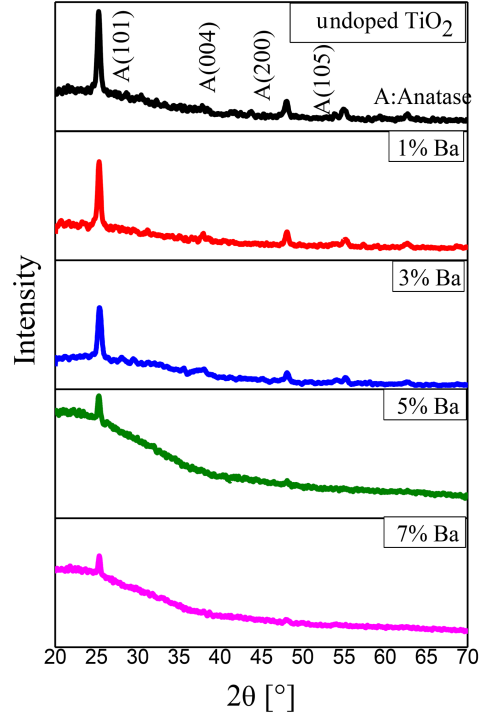


Fig. 1. XRD patterns of undoped and various Ba-doped TiO₂ thin films annealed at 550°C .

TABLE I

Structural parameters obtained from XRD patterns of Ba²⁺-doped TiO₂ thin films.

Samples	L [nm]	$\delta \times 10^{-4}$ [lines/m ²]	$\varepsilon \times 10^{-2}$
undoped TiO ₂	19	29.20	11.46
1% Ba	17	34.60	16.01
3% Ba	16	39.06	16.87
5% Ba	12	69.44	18.54
7% Ba	9	123.45	21.27

As shown in Table I, the crystallite size decreases with increasing Ba content, indicating the deterioration of the film crystallinity. This can be explained by the large difference between the ionic radius of Ti⁴⁺ (0.68 Å) and Ba⁺² (1.61 Å). The incorporation of barium into the TiO₂ matrix induces pressure inside the TiO₂ unit cell and thus increases the number of defects and inhibits crystals growth, which in turn decreases both the crystalline and crystallite size of Ba-doped TiO₂ films [14].

In addition, the dislocation density (δ) and the strain (ε) in the films have been determined using [15]

$$\delta = \frac{1}{L^2}, \quad (2)$$

and

$$\varepsilon = \frac{\beta \cos(\theta)}{4}, \quad (3)$$

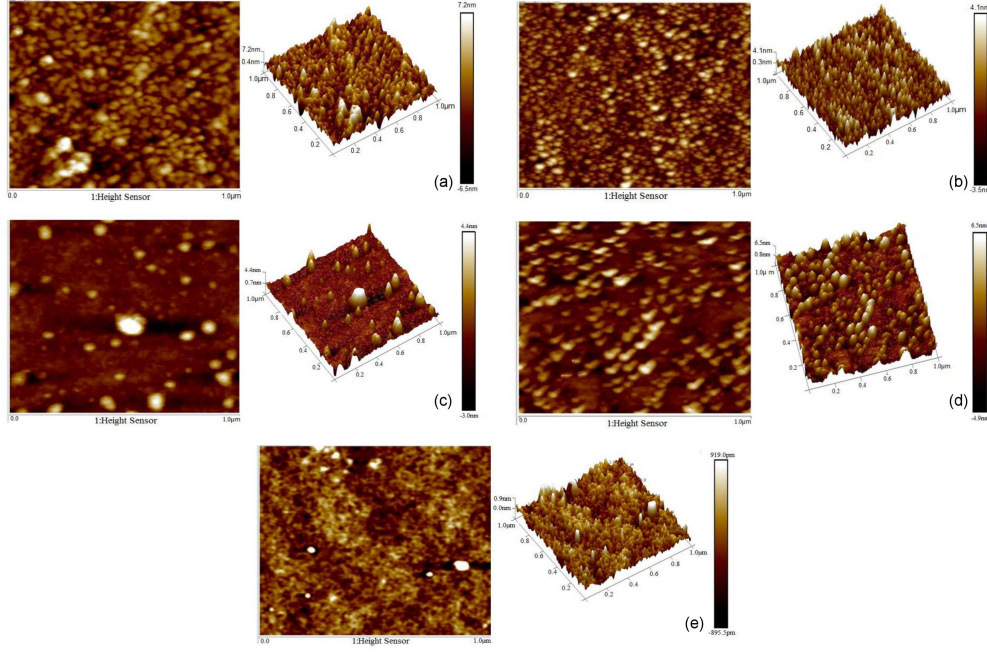


Fig. 2. 2D and 3D AFM micrographs of TiO_2 thin films as a function of Ba content: (a) undoped TiO_2 , (b) 1% Ba, (c) 3% Ba, (d) 5% Ba, (e) 7%Ba.

respectively. According to Table I, we observe that both the dislocation density δ and strain ε in the films were increased by increasing the concentration of Ba. This may be another cause of the deterioration of the crystalline structure.

3.2. Surface morphology

The AFM images of the undoped and Ba-doped TiO_2 thin films annealed at 550°C for 2 h are shown in Fig. 2. A granular and porous surface can be observed. Further, with increasing Ba content, we observe a decrease in the average grain size and a change in topography. According to AFM micrographs, 3% Ba-doped TiO_2 films have the highest porous surface, resulting in a large specific surface area.

The roughness mean square (RMS) of the films decreased between 16.3 nm and 5.27 nm (Table II) as a function of the Ba doping. This may be due to the decrease of crystallite size and variation surface morphology. The decrease of roughness and the existence of pores in the surface of the films would influence the photocatalytic degradation properties of TiO_2 thin films.

3.3. Optical properties

The transmittance properties of undoped and Ba-doped TiO_2 thin films deposited on glass substrates and annealed at 550°C were examined using UV-vis in a spectral range between 300 and 800 nm wavelength range. The transmittance results are reported in Fig. 3, where the average transmittance higher than 75% occur for all the thin films in the visible region. The spectra reveal very pronounced

TABLE II

Gap energy (E_g), surface roughness (RMS) of Ba-doped TiO_2 thin films.

Samples	E_g [eV]	RMS [nm]	Thickness [nm]
undoped TiO_2	3.42	16.3	175
1% Ba	3.45	12.7	174
3% Ba	3.68	9.82	176
5% Ba	3.72	8.05	173
7% Ba	3.77	5.27	174

interference effects. The appearance of interferences indicates that our films are sufficiently thick. We also note that the deposited thin films begin to absorb between 300 and 350 nm, i.e., in the near ultraviolet. The absorption threshold shifts towards shorter wavelengths as the Ba concentrations increase. This indicates an increase in the gap of the TiO_2 films, and we calculated it using the Tauc formula [16, 17]

$$(\alpha h\nu)^2 = A(h\nu - E_g), \quad (4)$$

where α is the absorption coefficient, A is the constant, $h\nu$ is the photon energy, h is Planck's constant, and E_g is the optical band-gap. When $(\alpha h\nu)^2 = 0$, $E_g = h\nu$, an extrapolation of the linear region of the plot of $(\alpha h\nu)^2$ versus photon energy ($h\nu$) on the x -axis gives the value of the optical band gap. Figure 4 shows the extrapolations of the curves $(\alpha h\nu)^2$ as a function of $h\nu$. The obtained values are listed in Table II.

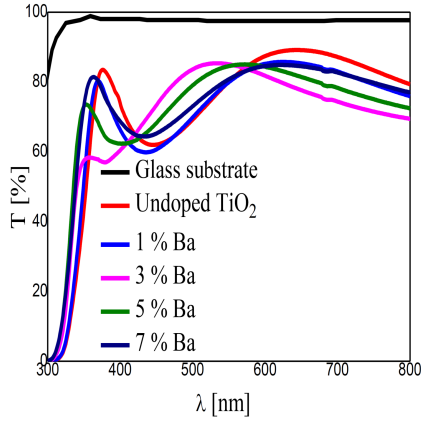


Fig. 3. Transmittance spectra of undoped and Ba-doped TiO₂ thin films.

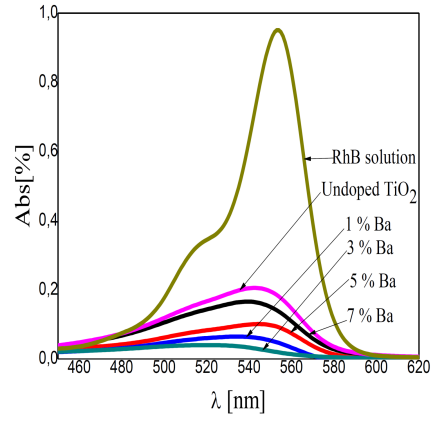


Fig. 5. Absorption spectra of RhB solution after 180 min of illumination in the presence of undoped and Ba-doped TiO₂ thin films and the absorption spectrum of RhB taken initially.

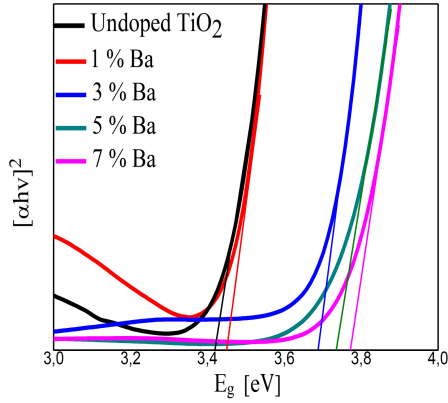


Fig. 4. The extrapolation of the curves $(\alpha h\nu)^2$ as a function of photon energy $h\nu$ of undoped and Ba-doped TiO₂ thin films.

It can be noted that the band gap of TiO₂ thin film gradually increases from 3.42 to 3.77 eV as a function of the Ba dopant. Vijayalakshmi and Sivaraj [18] and Gülen [19] also reported that the TiO₂ band gap increased with Ba dopant. The donor Ba atoms provide additional carriers, causing the Fermi level to shift towards the conduction band and, therefore, the band gap widens.

These spectra were also used to estimate the films' thicknesses using the envelope method [20]. The corresponding values are listed in Table II. As a result, the thicknesses were discovered to be unaffected by the barium content.

3.4. Photocatalytic properties

Figure 5 shows the absorption spectra of RhB after exposure to a UV light source during 180 min using undoped and 1%, 3%, 5%, 7% Ba-doped TiO₂ films. It can be seen that the RhB peak at 554 nm (wavelength) gradually decreases as a function of Ba content, with the 3% of Ba²⁺ doping showing a significant decrease compared to the rest.

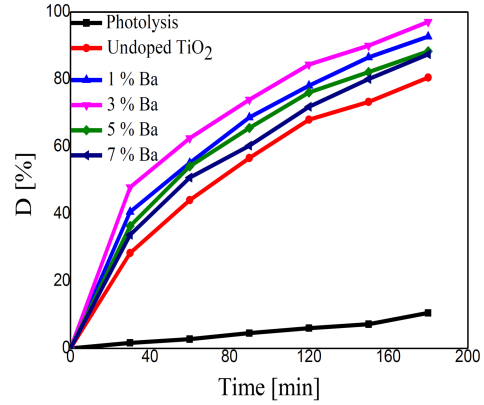


Fig. 6. Degradation rate of RhB in the presence of undoped and Ba-doped TiO₂ thin films at different irradiation time intervals.

In addition, the photodegradation rate D [%] was calculated according to [21]

$$D = \frac{C_0 - C_t}{C_0} \times 100, \quad (5)$$

where C_0 is the initial concentration and C_t is the concentration at different time.

Figure 6 shows the degradation rate D [%] of RhB solution in the presence of undoped and Ba-doped TiO₂ samples under UV light irradiation for 180 min. The degradation of RhB without TiO₂ or Ba-doped TiO₂ under UV light shows that the RhB molecule is not affected by UV light. On the other hand, the degradation rates were 77%, 93%, 98%, 89% and 84% in the presence of 0%, 1%, 3%, 5% and 7% of Ba-doped TiO₂ films, respectively. These results indicate an improvement in the photocatalytic activity with an increase in the Ba content. It also shows that the 3% Ba TiO₂ films display the most enhanced performance in the elimination of RhB.

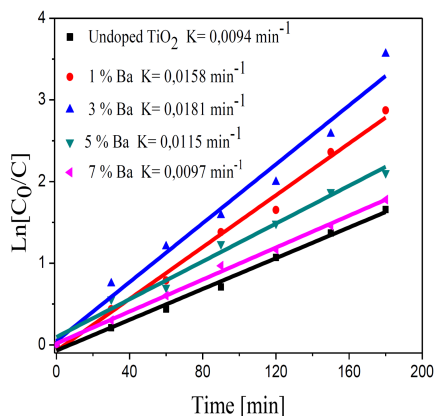


Fig. 7. The $\ln(C_0/C)$ results of RhB versus time.

The photocatalytic degradation is a pseudo first order reaction and its rate constant (k) can be calculated using [22]

$$\ln\left(\frac{C_0}{C}\right) = kt, \quad (6)$$

where k is the apparent rate constant [min^{-1}] and t is the irradiation time [min].

Figure 7 shows the relation (C_0/C) versus t , and the values of the rate constants were obtained from the slope of each curve. We note that the rate constant k increases with the increase of the Ba doping and the 3% of Ba-doped TiO_2 has the highest value. This result indicates that more Ba reduces the photocatalytic activity.

When a semiconductor oxide TiO_2 is exposed to UV light with an energy greater than the band gap, TiO_2 produces electrons (e^-) in the conduction band (BC) and holes (h^+) in the valence band (VB). These electrons can be captured by oxygen molecules adsorbed on the surface, forming a superoxide ion ($\bullet\text{O}_2^-$) or H_2O_2 , meanwhile holes can oxidize H_2O to hydroxyl radicals ($\bullet\text{OH}$) or O_2 . These powerful reactive radicals contribute to the decomposition of organic dye molecules adsorbed on the TiO_2 surface into CO_2 and H_2O [23, 24]. In this work, the increase of photocatalytic activity of Ba-doped TiO_2 films may be related to:

1. The decrease of crystal size of TiO_2 particles resulting in an increase of surface area and thus more active sites for reactant molecules.
2. The ability of Ba dopant to act as electron traps reducing the hole-electron pair recombination and leaving the photogenerated holes available for reaction with hydroxyl ions present in water to form OH^- radicals.
3. From AFM analysis, the 3% of Ba-doped TiO_2 samples showed a higher number of pores. RhB pollutant molecules can find more photoactive TiO_2 sites and suffer from photoinduced degradation [25, 26].

4. Conclusion

According to XRD analysis, all samples (undoped and Ba-doped TiO_2 thin films) show pure anatase phase. With increased barium content, the crystallinity and grain sizes of as-prepared samples decreased. The AFM observation shows clearly that the Ba doping affects the shape of TiO_2 . According to UV-vis analysis, the optical band gap increases with increasing barium content and photocatalytic activity of TiO_2 thin film. And, the 3% of Ba-doped TiO_2 was the best photocatalyst of RhB solution.

References

- [1] D.S.C. Halin, K.A. Razak, A. Azani, M.M.A.B. Abdullah, M.A.A.M. Salleh, N. Mahmed, M.M. Ramli, A.W. Azhari, V. Chobpattana, Ł. Kaczmarek, *Acta Phys. Pol. A* **138**, 159 (2020).
- [2] J.A. Borrego Pérez, M. Courel, M. Pal, F. Paraguay Delgado, N.R. Mathews, *Ceram. Int.* **43**, 15777 (2017).
- [3] S. Bouattour, W. Kallel, A.M. Botelho do Rego, L.F. Vieira Ferreira, I. Ferreira Machado, S. Boufi, *Appl. Organometal. Chem.* **24**, 692 (2010).
- [4] F. Abbas, R. Bensaha, *Optik* **247**, 167846 (2021).
- [5] Y.-H. Zhang, A. Reller, *J. Mater. Chem.* **11**, 2537 (2001).
- [6] M. Kang, *J. Mol. Catal. A Chem.* **197**, 173 (2003).
- [7] N. Nogishi, T. Iyoda, K. Hashimoto, A. Fujishima, *Chem. Lett.* **9**, 841 (1995).
- [8] K. Kato, A. Tsuzuki, Y. Torii, H. Taoda, T. Kato, Y. Butsungan, *Mater. Sci.* **30**, 2259 (1998).
- [9] R.S. Sonawane, B.B. Kale, M.K. Dongare, *Mater. Chem. Phys.* **85**, 52 (2004).
- [10] Z. Wang, U. Helmersson, P.O. Kall, *Thin Solid Films* **405**, 50 (2002).
- [11] H. Bensouyad, H. Sedrati, H. Dehdouh, M. Brahimi, F. Abbas, H. Akkari, R. Bensaha, *Thin Solid Films* **519**, 96 (2010).
- [12] R. Mechiakh, F. Meriche, R. Kremer, R. Bensaha, B. Boudine, A. Boudrioua, *Opt. Mater.* **30**, 645 (2007).
- [13] L. Alexander, H.P. Klug, *Appl. Phys.* **21**, 137 (1950).
- [14] F.B. Li, X.Z. Li, M.F. Hou, *Appl. Catal. B Environ.* **48**, (2004).
- [15] K. Mageshwari, R. Sathyamoorthy, *Mater. Sci. Semicond. Proc.* **16**, 337 (2013).
- [16] M. Lixiang, H. Chunming, W. Dawei, Z. Zhiguang, W. Yinyue, *Appl. Surf. Sci.* **255**, 9285 (2009).

- [17] S. Mahanty, S. Roy, S. Sen, *J. Cryst. Growth* **261**, 77 (2004).
- [18] K. Vijayalakshmi, D. Sivaraaj, *J. R. Soc. Chem.* **6**, 9663 (2016).
- [19] Y. Gülen, *Acta Phys. Pol. A* **126**, 763 (2012).
- [20] J. Yu, G. Wang, B. Cheng, M. Zhou, *Appl. Catal. B Environ.*, **69** 171 (2007).
- [21] K.K. Behzad, S.M. Rasoul, *Mater. Res. Bull.* **47**, 362 (2012).
- [22] N.R. Mathews, E.R. Morales, M.A. Cortes-Jacome, J.A. Toledo Antonio, *Sol. Energy* **83**, 1499 (2009).
- [23] Y.F. Tu, S.Y. Huang, J.P. Sang, X.W. Zou, *J. Alloys. Compd.* **482**, 382 (2009).
- [24] I.K. Konstantinou, T.A. Albanis, *Appl. Catal. B* **49**, 1 (2004).
- [25] O. Beldjebli, R. Bensaha, Y. Selim Ocak, L. Amirache, R. Boukherroub, *Mater. Res. Express* **6**, 085036 (2019).
- [26] A. Aouina, F. Bensouici, M. Bououdina, R. Tala-Ighil, M. Toubane, F. Kezzoula, K. Chebout, *Mater. Res. Express* **6**, 16406 (2019).
- [27] E. Cerro-Prada, M. Manso, V. Torres, J. Soriano, *Front. Struct. Civil Eng.* **10**, 189 (2016).